ACS APPLIED MATERIALS & INTERFACES

Research Article

www.acsami.org

Templating and Charge Injection from Copper Electrodes into Solution-Processed Organic Field-Effect Transistors

Chang Hyun Kim,*[,†] Htay Hlaing,[‡] Fabio Carta,[‡] Yvan Bonnassieux,[†] Gilles Horowitz,[†] and Ioannis Kymissis*[,‡]

[†]LPICM, Ecole Polytechnique, CNRS, 91128 Palaiseau, France

[‡]Department of Electrical Engineering, Columbia University, New York, New York 10027, United States

ABSTRACT: Solution-processed organic field-effect transistors (OFETs) using chemically modified copper electrodes are reported. The purpose of this study is to shed light on the use of inexpensive copper electrodes in bottom-contact OFETs, which is consistent with the major goal of organic electronics: the realization of low-cost electronics. 6,13-Bis(triisopropylsilylethynyl)pentacene was used for solution-processed hole-transporting molecular films and pentafluorobenzenethiol was used to form self-assembled monolayers (SAMs) on the contact metals. We conducted a comparative study on copper and gold contacts and realized that, under the same performance improvement schemes, via SAM treatment and controlled crystal growth, the copper electrode device experienced a more significant enhancement than the gold electrode device. We attribute the beneficial effects of SAMs to the improved charge injection and transport properties, which are critical double effects from the fluorinated aromatic SAM structure. Grazing-incidence wide-angle X-ray scattering (GIWAXS) measurements showed that templating property of SAMs promotes the crystallization of TIPS-pentacene films at the metal/organic interface. The presented result indicates that copper can be regarded as a promising candidate for reducing the use of gold in organic-based circuits and systems, where the cost-effective production is an important issue.

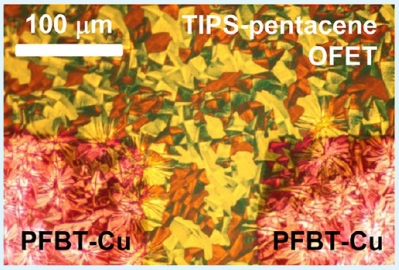

KEYWORDS: *organic field-effect transistors (OFETs), copper electrodes, self-assembled monolayers (SAMs), charge-carrier injection, crystallization, TIPS-pentacene*

INTRODUCTION

Organic field-effect transistors (OFETs) are experiencing continuous improvement in performance and offer new opportunities for flexible, lightweight, large-area displays and microelectronic systems.[1−3] The recent development of stable, high-performance soluble organic semiconductors enables organic electronics to steadily proceed toward the goal of low-cost electronics, which takes maximum advantage of inexpensive solution-based deposition techniques.[4,5] Despite the obvious orientation toward a low-cost technology, the precious metal gold is still a predominant choice for source/drain electrodes in OFETs, because of its chemical inertness, high electrical conductivity, processability, and ability to form a low-injection-barrier junction with most *p*-type organic semiconductors.[6] In addition to these inherently outstanding properties of gold, the demonstration of OFET performance improvement by formation of self-assembled monolayers (SAMs) on the gold surface[7,8] has opened up the possibilities of tuning contact energetics and controlling film morphology at the metal/organic interface, further solidifying the position of gold as the most popular metal electrode in OFETs.[9,10]

Surprisingly, reducing the use of gold has been of only minor interest in OFET research, despite its potential cost impact. Several groups have recently addressed this issue and drawn attention to copper as an alternative.[11−13] Copper is the most extensively used metal for cables, wires, and electrical contacts, because of its high conductivity and low cost.[14,15] The favorable work function of copper for both hole and electron injection, as well as its well-established processability and the availability of printable copper-containing inks,[16] are other attractive features for OFETs. In the literature, a small number of reports have addressed Cu-electrode OFETs in the bottom-gate top-contact architecture, which shows fairly good performance.[12,13,17,18] Physically, this staggered top-contact geometry takes advantage of large injection area[19] and continuous channel carrier distribution[20] and is thus expected to exhibit the best transport property of a given semiconductor without serious contact-related problems. For large-scale integrated circuits, however, the bottom-contact structure is more suitable, because of its compatibility with the lithographical patterning of electrodes prior to semiconductor deposition. Di and co-workers have suggested chemically modified bottom Cu electrodes with the charge-transfer complex Cu-tetracyanoquinodimethane (Cu-TCNQ) for pentacene,[11] rubrene, tetracyanoquinodimethane (TCNQ), and copper phthalocyanine (CuPc) transistors.[21] These results point out the functionalization of Cu electrodes as a promising approach for high-performance copper bottom-contact OFETs.

Here, we report on the solution-processed 6,13-bis-(triisopropylsilylethynyl)pentacene (TIPS-pentacene) transis-

Received: January 24, 2013
Accepted: April 12, 2013
Published: April 12, 2013

tors with Cu bottom electrodes modified by pentafluorobenzenethiol (PFBT) SAMs (Figure 1). To the best of our knowledge, this is the first attempt to match Cu electrodes with a solution-processed organic semiconductor and also the first demonstration of SAM-treated Cu electrodes in OFETs. It is found that PFBT modification results in significant performance improvement to copper bottom-contact OFETs, bringing them within an order of magnitude to the transconductance found in Au-electrode devices fabricated under an identical process. In this work, we examine both spin-cast and directionally grown TIPS-pentacene films. The spin-cast film reveals the crystal-templating properties of the SAM-treated electrodes. We also apply a directional drying crystal growth method to creating TIPS-pentacene grains. These devices permit examination of charge-transport anisotropy of the TIPS-pentacene thin films and grain-boundary effects.

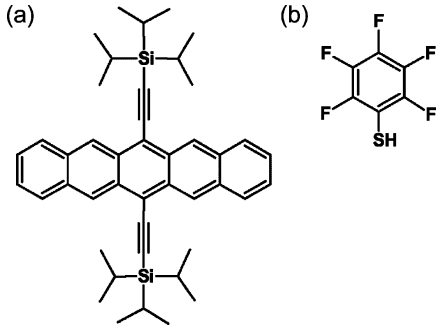

Figure 1. Chemical structure of (a) 6,13-bis(triisopropylsilylethynyl)-pentacene (TIPS-pentacene) and (b) pentafluorobenzenethiol (PFBT).

EXPERIMENTAL SECTION

Device Fabrication and Characterization. Bottom-gate, bottom-contact OFETs were fabricated on a heavily doped *p*-type Si wafer with a 300-nm thermal oxide layer, which serves as a common gate electrode/gate dielectric structure. The substrates were ultrasonically cleaned with acetone and isopropanol. With a 5-nm chromium adhesion layer, 50-nm Au or Cu source/drain electrodes were deposited by thermal evaporation. For SAM formation on electrodes, selected samples were immersed in a 10 mM PFBT solution in isopropanol for 30 min, followed by rinsing with pure isopropanol and blow drying with nitrogen. All samples were treated with hexamethyldisilazane (HMDS) for reduced trap states at the semiconductor/insulator interface, by spin-coating a neat HMDS solution at 3000 rpm for 1 min. TIPS-pentacene solution was prepared at a concentration of 15 mg/mL in 1,2-dichlorobenzene. For spin-cast TIPS-pentacene films, we used a spin seed of 1000 rpm for 30 s, followed by an annealing step at 100 °C for 30 min. For textured TIPS-pentacene films, the substrate was covered with drop-cast TIPS-pentacene solution and immediately moved onto a tilted drying stage for a desired directional growth, where the samples were left at 100 °C for 1 h for complete drying of the solvent-rich films. Current−voltage characteristics of the as-fabricated devices were recorded using a Keithley Model 4200 semiconductor characterization system.

Opitical Microscopic Analysis. Optical microscopic images were taken using a Nikon Eclipse E600FN microscope under crossed polarizers, coupled with a Canon Rebel T1i EOS 500D digital camera.

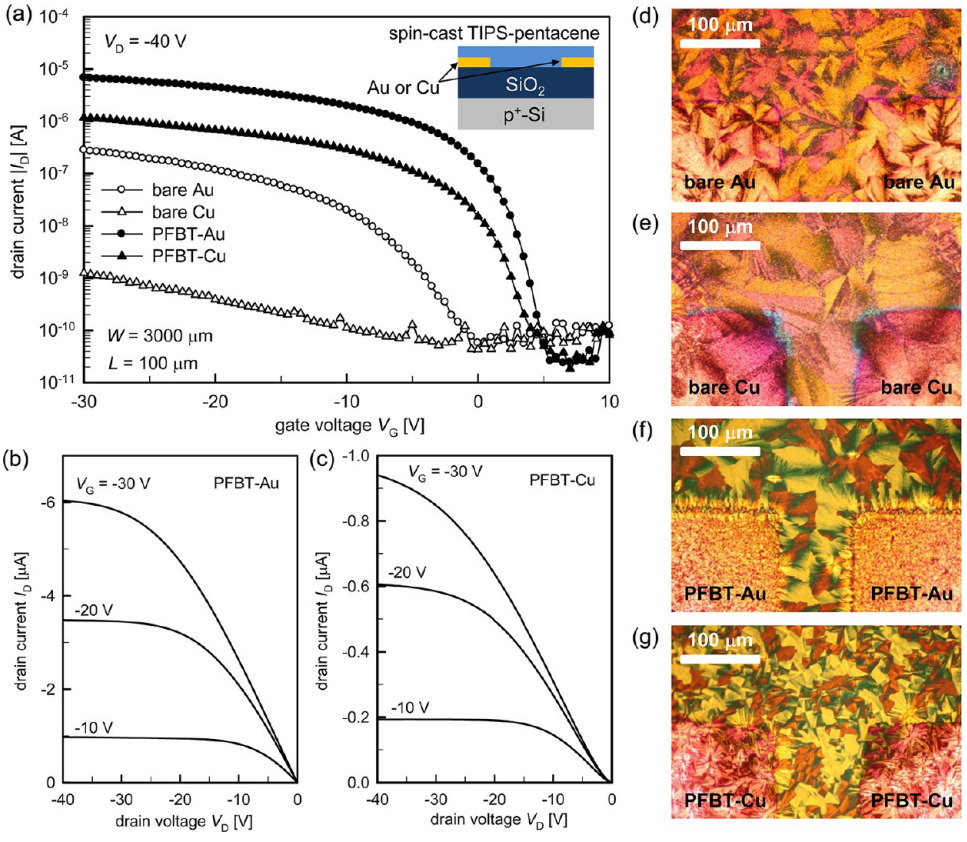

Figure 2. Electrical and morphological characteristics of the spin-cast TIPS-pentacene transistors showing the effect of SAM treatment: (a) comparison of the transfer characteristics (inset shows the device structure; W is the channel width and L is the channel length); (b,c) output characteristics of the transistors with PFBT-treated electrodes ((b) PFBT-Au and (c) PFBT-Cu); and (d−g) polarized optical microscopic images on the TIPS-pentacene films at the near-electrode region ((d) bare gold, (e) bare copper, (f) PFBT-Au, and (g) PFBT-Cu).

dx.doi.org/10.1021/am400325k | ACS Appl. Mater. Interfaces 2013, 5, 3716−3721

Grazing-Incidence Wide-Angle X-ray Scattering (GIWAXS) Measurement. Grazing-incidence wide-angle X-ray scattering (GIWAXS) measurements were carried out at the X9 undulator-based beamline at the National Synchrotron Light Source (NSLS) at Brookhaven National Laboratory. The incident X-ray beam (λ = 0.09184 nm) was collimated using slits and focused onto the sample position using Kirkpatrick–Biaz mirrors. This provides a spot 100 μm (width) × 80 μm (height) at the sample position whose footprint along the sample spreads out by the inverse incident angle. The sample stage was located inside the vacuum chamber (pressure ≈ 40 Pa), where both the incident angle and sample translation are computer-controlled. A two-dimensional (2-D) charged-coupled device (CCD) detector was positioned ~270 mm from the center of the sample stage to collect the GIWAXS images inside the same vacuum chamber. Data conversion to q-space was accomplished by calibration, using silver behenate powder.

RESULTS AND DISCUSSION

Spin-Cast OFETs. We first examined the influence of PFBT SAMs on thin-film morphology and transistor performance. Figure 2a shows that the chemical treatment on both Au and Cu electrodes significantly improves the performance of spin-cast TIPS-pentacene transistors, in terms of the on-to-off current ratio and field-effect mobility (μ_{FE}). The extracted mobility values will be given and discussed in more detail hereinafter. Note here that the Cu-electrode devices experience a particularly significant enhancement. We infer that the performance improvement comes from the double effect of PFBT; the SAM provides both for a reduction in the injection barrier and a crystallization of TIPS-pentacene. These two effects simultaneously improve the transistor charge injection and transport properties.

An interface dipole layer can significantly change the contact energetics and also affect the chemical interaction at a metal/organic interface.[22] As described in our previous study,[23] the electron-withdrawing character of fluorine provides the PFBT monolayer with a strong dipole moment that points downward to the metal substrate. This arrangement leads to an increase in the metal work function, compared to an untreated surface. Although no direct measurement of the energy levels was conducted in the present study, we can refer to the recent reports on the work functions of PFBT-treated electrodes. Table 1 shows that the work function change of copper by PFBT SAMs reaches +0.8 eV, which makes the PFBT-Cu electrode a good hole-injecting contact into the highest occupied molecular orbital (HOMO) level of TIPS-pentacene. Therefore, improved charge-carrier injection is the first reason for the spectacular improvement of our Cu-electrode OFET characteristics. However, the slight upward bending at low drain voltage (V_D) in the output curves of the PFBT-Cu device in Figure 2c shows that contact resistance problem still exists at the source/channel edge.[27] Note that the output curves of the PFBT-Au device in Figure 2b have almost-ideal linear-regime characteristics. Despite significant improvement, the work function of PFBT-Cu is still lower than that of PFBT-Au (Table 1) and it accounts for the fact that a contact resistance is still present.

Table 1. Literature Values of the Properties of Gold and Copper

property	Value	
	Au	Cu
electrical conductivity at 300 K[a]	4.403 × 10^5 S/cm	5.797 × 10^5 S/cm
work function of the atomically clean surface[a]	5.31–5.47 eV	4.48–5.10 eV
work function of the air-exposed surface[b]	4.7–4.9 eV	4.65 eV
work function of the PFBT-treated surface[c]	5.7–5.9 eV	5.45 eV

[a]Data taken from ref 14. [b]Data taken from refs 24–26. [c]Data taken from refs 25 and 26.

The morphological effect is revealed by the polarized optical microscopic images shown in Figures 2d–g. The PFBT-treated samples exhibit a distinctive morphology in the electrode region, whereas the untreated samples show undistinguishable or continuous morphology in both the electrode and the insulator regions. Although less pronounced in the PFBT-Cu sample, Figures 2f and 2g show that the characteristic morphology of the electrode region slightly extends toward the insulator region, which bears a resemblance to the images reported by Jurchescu and co-workers on fluorinated 5,11-bis(triethylsilylethynyl)anthradithiophene (diF-TESADT) films deposited on PFBT-Au electrodes.[4,28–30] To explain this effect, these authors put forward the so-called "contact-induced crystallization" phenomenon that leads to a well-ordered organic layer at the near-electrode region. It should be noted here that the "driving force" for the contact-crystallization effect on diF-TESADT is generally attributed to the sulfur–fluorine reaction between PFBT and diF-TESADT, which is also known to promote the molecular packing of diF-TESADT.[4,30] Even if similar contact-induced crystallization takes place for TIPS-pentacene, its origin cannot be the same type of reaction, because of the absence of S or F atoms in its molecular structure (Figure 1a). It is thus reasonable to infer that the main origin of the contact-induced crystallization of TIPS-pentacene by PFBT-treated electrodes is the so-called "templating effect", which is regarded as a characteristic of aromatic SAMs.[9,10,31] A well-ordered PFBT monolayer on a gold or copper surface forms a two-dimensional (2-D) structure of periodically positioned upright benzene rings, which serve as a template for the growth of TIPS-pentacene crystallites.

Grazing-Incidence Wide-Angle X-ray Scattering (GIWAXS). In order to further investigate the morphological aspect, we carried out structural analysis of the TIPS-pentacene films in the PFBT-treated Au and Cu samples by means of GIWAXS measurement.[32,33] Figures 3a–d show the 2-D GIWAXS pattern of the TIPS-pentacene films on the electrode and insulator regions of the PFBT-Au and PFBT-Cu samples. Strikingly well-defined peaks centered along the out-of-plane q_z-direction are observed in all four images, thus indicating that TIPS-pentacene is highly crystalline with a preferred orientation corresponding to lattice planes parallel to the substrate. The main peaks that appear along the q_z-direction at q_{xy} = 0 (see Figure 3e) can be identified by referring to the triclinic lattice structure of TIPS-pentacene.[34] As illustrated in Figure 3f, the (001) peak corresponds to the "edge-on" orientation with a π–π stacking direction that favors the charge-transport in OFETs, while "face-on" crystallites that give rise to the (111) peak do not contribute to the in-plane charge transport. From the peak positions estimated in Figure 3e, we extract two characteristic q_z components: q_{001} = 3.95 nm^{-1} and q_{111} = 9.82 nm^{-1}. These components correspond to the interplanar spacings $d_{001} = 2\pi/q_{001}$ = 1.59 nm and $d_{111} = 2\pi/q_{111}$ = 0.64 nm, which are close to the values calculated from the lattice parameters of the TIPS-pentacene single crystal[34] and thin film.[35] The profiles in Figure 3e clearly show that the

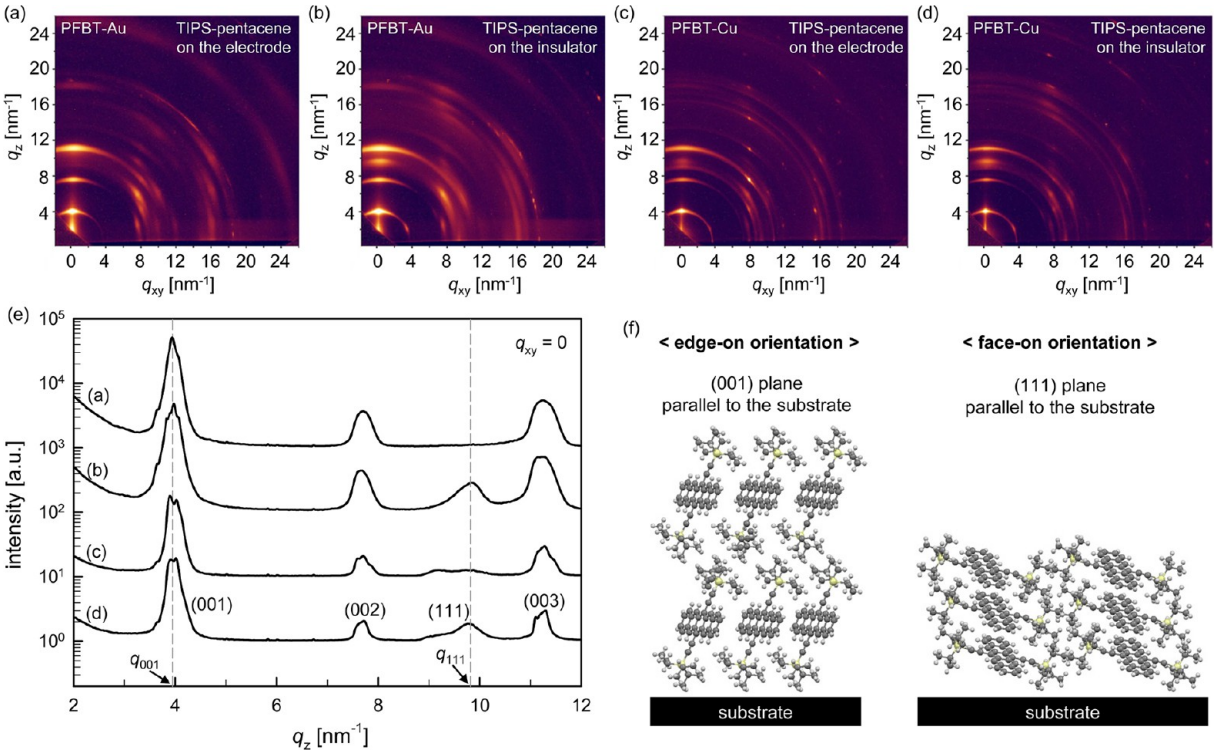

Figure 3. Two-dimensional (2-D) GIWAXS patterns of the spin-cast TIPS-pentacene films on (a) the electrode region in the PFBT-Au sample, (b) the insulator region in the PFBT-Au sample, (c) the electrode region in the PFBT-Cu sample, and (d) the insulator region in the PFBT-Cu sample. (e) Scattering profiles along the q_z-axis at q_{xy} = 0. Each profile is labeled by the corresponding 2-D GIWAXS image (Miller indices of the crystallographic planes are located at the corresponding peak position). (f) Two characteristic orientations of the TIPS-pentacene crystallites, with respect to the substrate.

electrodes are predominantly covered by well-ordered "edge-on" crystallites, whereas the "face-on" components are localized at the insulator or far-electrode regions. This finding, together with the optical images in Figures 2f and 2g, allows us to convincingly visualize the thin-film growth process. Mimicking the underlying PFBT templates, solution-cast TIPS-pentacene molecules principally nucleate on the electrodes; then, the growth extends outward upon evaporation of the solvent. Benefiting from this contact-templating effect, the conducting channel on the insulator mainly consists of desirable (001) crystallites with only locally existing (111) crystallites, which leads to the efficient charge-carrier transport through the molecular orbitals for transistor operation.

Textured OFETs. It is widely accepted that charge transport in a polycrystalline organic semiconductor is influenced by grain boundaries.[36,37] We realize that, despite an excellent crystallinity of the TIPS-pentacene films in the SAM-treated OFETs, the transport property can be seriously affected by grain boundaries, because of the relatively small grain sizes seen in Figures 2f and 2g. To examine the possibility of further performance improvement, we applied a directional growth method on the PFBT-modified gold and copper, by which highly textured elongated grains are obtained. The samples were dried on a tilted stage, which encourages drying in the downhill direction as the drop evaporates and recedes toward the low side. The growth direction is defined with respect to the source-to-drain direction (S-D), and its effect on the electrical characteristics and the thin-film morphology is shown in Figure 4. Figure 4a shows that, for both gold and copper, the films grown along S-D give better transistor performance than the films grown across S-D. The first reason for this tendency is the in-plane charge-transport anisotropy of TIPS-pentacene crystals.[34] Films grown along S-D mostly contain crystallites of which the $\pi-\pi$ stacking direction is more favorably aligned with the charge-transport direction, which, in turn, results in the higher charge-carrier mobility, compared to the films grown across S-D.[38] The second factor is the grain-boundary effect. In the case of growth along S-D, elongated single-crystal-like domains bridge the source and drain electrodes, as shown in Figures 4f and 4g. In contrast, many grain boundaries limit the source-to-drain current flow in the films grown across S-D, as shown in Figures 4d and 4e.

Performance Analysis. Table 2 summarizes the field-effect mobility (μ_{FE}) and threshold voltage (V_T) extracted from the transfer curves in Figures 2a and 4a, using the conventional extrapolation method of the saturation-regime square-root drain current.[1] Upon the two-step performance improvement scheme, first by SAM treatment and then by texturing, the μ_{FE} value of the Cu-electrode transistor increases from 1.3×10^{-5} cm^2/V s to 0.022 cm^2/V s, which is a factor more significant than that of the Au-electrode device. Comparing the best performance devices (PFBT-treated textured OFETs with the growth along S-D), the Au-electrode device has an apparent mobility only ~5 times higher than the Cu-electrode device, which is an impressive result when considering the cost difference. We also note that, comparing six PFBT-treated transistors, the μ_{FE} value of the spin-cast transistor roughly corresponds to the average μ_{FE} value of the textured transistors with different growth directions. Together with the corresponding optical images, this finding indirectly confirms that crystallites in the spin-cast films have random in-plane orientation with a substantial density of grain boundaries,

dx.doi.org/10.1021/am400325k | ACS Appl. Mater. Interfaces 2013, 5, 3716−3721

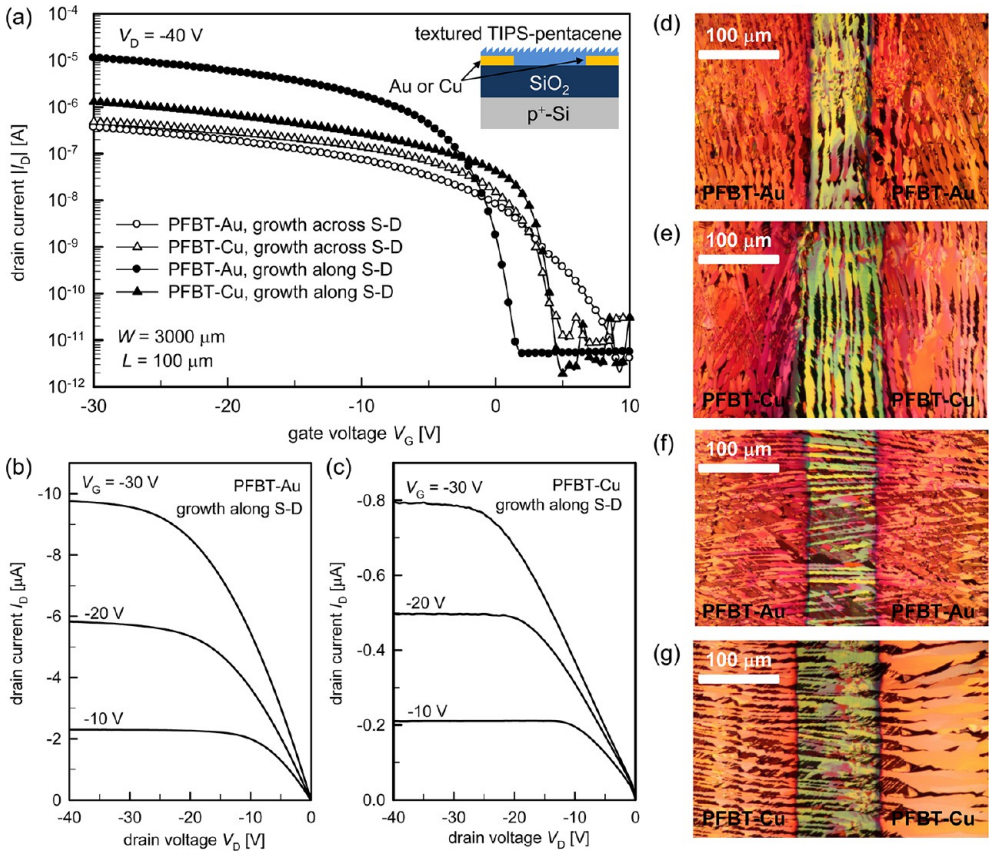

Figure 4. Electrical and morphological characteristics of the textured TIPS-pentacene transistors showing the effect of crystal-growth direction: (a) comparison of the transfer characteristics (inset shows the device structure); (b, c) output characteristics of the transistors with the laterally grown TIPS-pentacene films; (d–g) polarized optical microscopic images on the TIPS-pentacene films at the channel region ((d and e) growth across S-D, (f and g) growth along S-D).

Table 2. Summary of the Field-Effect Mobilities and Threshold Voltages Extracted from the Saturation Regime Transfer Curves

sample	field-effect mobility, μ_{FE} [$cm^2/V\ s$]	threshold voltage, V_T [V]
Spin-Casting		
bare Au	2.3×10^{-3}	−3.0
bare Cu	1.3×10^{-5}	−7.0
PFBT-Au	0.083	3.3
PFBT-Cu	0.010	3.0
Texturing		
PFBT-Au, growth across S-D	1.9×10^{-3}	5.0
PFBT-Cu, growth across S-D	5.6×10^{-3}	3.9
PFBT-Au, growth along S-D	0.12	−0.45
PFBT-Cu, growth along S-D	0.022	3.9

which macroscopically averages the transport properties of the homogeneously grown lateral and longitudinal grains.

We believe there is significant room for further performance improvement for PFBT-treated devices. Especially for spin-cast OFETs, low μ_{FE} values can be mainly attributed to the large channel length (L) of 100 μm. A series of works on spin-cast diF-TESADT OFETs with PFBT-Au showed that μ_{FE} increased by almost 2 orders of magnitude by reducing L from 100 μm down to 5 μm, because the crystallinity is worse in the middle-channel region than that in the near-electrode region.[4,29,30] Various process development schemes can be also applied, e.g., comparison among different solvents for TIPS-pentacene solution and following optimization steps on solution preparation and deposition conditions.[39] Maximizing the ordering of the SAMs on a metal surface is another important approach, which can be achieved by optimizing SAM preparation conditions, such as immersion temperature and time.[40,41]

Finally, we note a large positive shift of V_T in Table 2 after deposition of PFBT SAMs in spin-cast OFETs. The shift is as large as +6.3 V for Au and +10 V for Cu. The increased work function of gold or copper by PFBT modifies the flat-band voltage and tends to negatively shift V_T, but its contribution should remain under approximately −1 V (Table 1). Therefore, the V_T shift observed here should be dominated by the reduction of trap states by SAM_S. The V_T value in OFETs is sensitive to the interface trap density, because these states must be filled before a conducting channel is formed while the surface Fermi level approaches the transport orbital by applying a gate voltage (V_G).[20,42] The positive movement of V_T thus corresponds to an earlier formation of channel upon a V_G sweep from the off-state to the on-state. Accordingly, it shows that highly crystalline TIPS-pentacene films with SAMs contain a lower density of trap states, because of reduced structural defects and disorder.[43]

CONCLUSION

In conclusion, we demonstrate solution-processed organic field-effect transistors (OFETs) with self-assembled monolayer (SAM)-treated copper as source/drain bottom contacts. A significant performance improvement was observed for Cu-electrode transistors by pentafluorobenzenethiol (PFBT) SAM chemical modification and the controlled crystal growth. The effect of SAM was elucidated by improved charge-carrier injection and the crystal-templating property. The improved Cu-electrode device showed promising performance that approaches that of similar Au-electrode devices fabricated under similar conditions. We believe that this initial result can suggest the use of SAM-treated Cu electrodes for practical low-cost electronics and motivate further studies on exploring various SAM materials for copper and their application to different organic semiconductors.

AUTHOR INFORMATION

Corresponding Author

*E-mail: chang-hyun.kim@polytechnique.edu (C.H.K.); johnkym@ee.columbia.edu (I.K.).

Notes

The authors declare no competing financial interest.

ACKNOWLEDGMENTS

C.H.K. acknowledges the financial support from the Alliance Program Doctoral Mobility Grant and the Ecole Polytechnique Graduate School Mobility Grant. He also would like to thank the Vice Presidency for External Relations (DRE) in Ecole Polytechnique for his Ph.D. fellowship. I.K., H.H., and overall project coordination, as well as sample growth and characterization, were supported as part of the Center for Re-Defining Photovoltaic Efficiency through Molecular-Scale Control, an Energy Frontier Research Center funded by the U.S. Department of Energy (DOE), Office of Science, Office of Basic Energy Sciences (under Award No. DE-SC0001085). We would also like to thank Kevin Yager and the National Synchrotron Light Source (NSLS) at the Brookhaven National Laboratory for use of the X9 Beamline (No. DE-AC02-98CH10886) to acquire our X-ray scattering data.

REFERENCES

(1) Braga, D.; Horowitz, G. *Adv. Mater.* **2009**, *21*, 1473−1486.
(2) Klauk, H. *Chem. Soc. Rev.* **2010**, *39*, 2643−2666.
(3) Gelinck, G.; Heremans, P.; Nomoto, K.; Anthopoulos, T. D. *Adv. Mater.* **2010**, *22*, 3778−3798.
(4) Gundlach, D. J.; Royer, J. E.; Park, S. K.; Subramanian, S.; Jurchescu, O. D.; Hamadani, B. H.; Moad, A. J.; Kline, R. J.; Teague, L. C.; Kirillov, O.; Richter, C. A.; Kushmerick, J. G.; Richter, L. J.; Parkin, S. R.; Jackson, T. N.; Anthony, J. E. *Nat. Mater.* **2008**, *7*, 216−221.
(5) Arias, A. C.; MacKenzie, J. D.; McCulloch, I.; Rivnay, J.; Salleo, A. *Chem. Rev.* **2010**, *110*, 3−24.
(6) Kahn, A.; Koch, N.; Gao, W. *J. Polym. Sci., Part B: Polym. Phys.* **2003**, *41*, 2529−2548.
(7) Katz, H. E.; Johnson, J.; Lovinger, A. J.; Li, W. *J. Am. Chem. Soc.* **2000**, *122*, 7787−7792.
(8) Kymissis, I.; Dimitrakopoulos, C. D.; Purushothaman, S. *IEEE Trans. Electron Devices* **2001**, *48*, 1060−1064.
(9) DiBenedetto, S. A.; Facchetti, A.; Ratner, M. A.; Marks, T. J. *Adv. Mater.* **2009**, *21*, 1407−1433.
(10) Miozzo, L.; Yassar, A.; Horowitz, G. *J. Mater. Chem.* **2010**, *20*, 2513−2538.
(11) Di, C.-A.; Yu, G.; Liu, Y.; Xu, X.; Wei, D.; Song, Y.; Sun, Y.; Wang, Y.; Zhu, D.; Liu, J.; Liu, X.; Wu, D. *J. Am. Chem. Soc.* **2006**, *128*, 16418−16419.
(12) Wang, S. D.; Minari, T.; Miyadera, T.; Tsukagoshi, K.; Aoyagi, Y. *Appl. Phys. Lett.* **2007**, *91*, No. 203508.
(13) Li, J.; Zhang, X.-W.; Zhang, L.; Zhang, H.; Jiang, X.-Y.; Khizarul, H.; Zhu, W.-Q.; Zhang, Z.-L. *Synth. Met.* **2010**, *160*, 376−379.
(14) *CRC Handbook of Chemistry & Physics*, 93rd ed.; Haynes, W. M., Ed.; CRC Press/Taylor and Francis: Boca Raton, FL, 2012.
(15) *Copper and Copper Alloys*; Davis, J. R., Ed.; ASM International: Materials Park, OH, 2001.
(16) Hong, C. M.; Wagner, S. *IEEE Electron Device Lett.* **2000**, *21*, 384−386.
(17) Li, J.; Zhang, X.-W.; Zhang, L.; Zhang, H.; Jiang, X.-Y.; Zhu, W.-Q.; Zhang, Z.-L. *Semicond. Sci. Technol.* **2010**, *25*, No. 045027.
(18) Liang, Y.; Chang, H.-C.; Ruden, P. P.; Frisbie, C. D. *J. Appl. Phys.* **2011**, *110*, No. 064514.
(19) Street, R. A.; Salleo, A. *Appl. Phys. Lett.* **2002**, *81*, 2887−2889.
(20) Kim, C. H.; Bonnassieux, Y.; Horowitz, G. *IEEE Electron Device Lett.* **2011**, *32*, 1302−1304.
(21) Di, C.-A.; Yu, G.; Liu, Y.; Guo, Y.; Sun, X.; Zheng, J.; Wen, Y.; Wu, W.; Zhu, D. *Chem. Mater.* **2009**, *21*, 4873−4879.
(22) Hwang, J.; Wan, A.; Kahn, A. *Mater. Sci. Eng. R* **2009**, *64*, 1−31.
(23) Jia, Z.; Lee, V. W.; Kymissis, I.; Floreano, L.; Verdini, A.; Cossaro, A.; Morgante, A. *Phys. Rev. B* **2010**, *82*, No. 125457.
(24) Wan, A.; Hwang, J.; Amy, F.; Kahn, A. *Org. Electron.* **2005**, *6*, 47−54.
(25) Smith, J.; Hamilton, R.; Qi, Y.; Kahn, A.; Bradley, D. D. C.; Heeney, M.; McCulloch, I.; Anthopoulos, T. D. *Adv. Funct. Mater.* **2010**, *20*, 2330−2337.
(26) Schmidt, C.; Witt, A.; Witte, G. *J. Phys. Chem. A* **2011**, *115*, 7234−7241.
(27) Kim, C. H.; Bonnassieux, Y.; Horowitz, G. *IEEE Trans. Electron Devices* **2013**, *60*, 280−287.
(28) Jurchescu, O. D.; Hamadani, B. H.; Xiong, H. D.; Park, S. K.; Subramanian, S.; Zimmerman, N. M.; Anthony, J. E.; Jackson, T. N.; Gundlach, D. J. *Appl. Phys. Lett.* **2008**, *92*, No. 132103.
(29) Kline, R. J.; Hudson, S. D.; Zhang, X.; Gundlach, D. J.; Moad, A. J.; Jurchescu, O. D.; Jackson, T. N.; Subramanian, S.; Anthony, J. E.; Toney, M. F.; Richter, L. J. *Chem. Mater.* **2011**, *23*, 1194−1203.
(30) Li, R.; Ward, J. W.; Smilgies, D.-M.; Payne, M. M.; Anthony, J. E.; Jurchescu, O. D.; Amassian, A. *Adv. Mater.* **2012**, *24*, 5553−5558.
(31) Tulevski, G. S.; Miao, Q.; Afzali, A.; Graham, T. O.; Kagan, C. R.; Nuckolls, C. *J. Am. Chem. Soc.* **2006**, *128*, 1788−1789.
(32) Hlaing, H.; Lu, X.; Hofmann, T.; Yager, K. G.; Black, C. T.; Ocko, B. M. *ACS Nano* **2011**, *5*, 7532−7538.
(33) Lu, X.; Hlaing, H.; Germack, D. S.; Peet, J.; Jo, W. H.; Andrienko, D.; Kremer, K.; Ocko, B. M. *Nat. Commun.* **2012**, *3*, 795.
(34) Anthony, J. E.; Brooks, J. S.; Eaton, D. L.; Parkin, S. R. *J. Am. Chem. Soc.* **2001**, *123*, 9482−9483.
(35) Mannsfeld, S. C. B.; Tang, M. L.; Bao, Z. *Adv. Mater.* **2011**, *23*, 127−131.
(36) Horowitz, G. *Adv. Funct. Mater.* **2003**, *13*, 53−60.
(37) Bolognesi, A.; Berliocchi, M.; Manenti, M.; Di Carlo, A.; Lugli, P.; Lmimouni, K.; Dufour, C. *IEEE Trans. Electron Devices* **2004**, *51*, 1997−2003.
(38) Chen, J.; Tee, C. K.; Shtein, M.; Martin, D. C.; Anthony, J. *Org. Electron.* **2009**, *10*, 696−703.
(39) Kim, C. S.; Lee, S.; Gomez, E. D.; Anthony, J. E.; Loo, Y.-L. *Appl. Phys. Lett.* **2008**, *93*, 103302.
(40) Kang, H.; Lee, N.-S.; Ito, E.; Hara, M.; Noh, J. *Langmuir* **2010**, *26*, 2983−2985.
(41) Azzam, W.; Bashir, A.; Ulrich Biedermann, P.; Rohwerder, M. *Langmuir* **2012**, *28*, 10192−10208.
(42) Braga, D.; Horowitz, G. *Appl. Phys. A* **2009**, *95*, 193−201.
(43) Kalb, W. L.; Haas, S.; Krellner, C.; Mathis, T.; Batlogg, B. *Phys. Rev. B* **2010**, *81*, No. 155315.